

Pressure-induced transitions in the 1-dimensional vanadium oxyhydrides $\text{Sr}_2\text{VO}_3\text{H}$ and $\text{Sr}_3\text{V}_2\text{O}_5\text{H}_2$, and comparison to 2-dimensional SrVO_2H

Takafumi Yamamoto,^{†,‡} Harry W. T. Morgan,[¶] Dihao Zeng,[¶] Takateru Kawakami,[§] Midori Amano Patino,[¶] Michael A. Hayward,^{*,¶} Hiroshi Kageyama,^{*,†,||} and John E. McGrady^{*,¶}

[†]*Department of Energy and Hydrocarbon Chemistry, Graduate School of Engineering, Kyoto University, Nishikyo-ku, Kyoto 615-8510, Japan*

[‡]*Laboratory for Materials and Structures, Tokyo Institute of Technology, Yokohama, Kanagawa, 226-8503, Japan*

[¶]*Department of Chemistry, University of Oxford, South Parks Road, Oxford OX1 3QR, U.K.*

[§]*Department of Physics, College of Humanities and Sciences, Nihon University, Setagaya, Tokyo 156-8550, Japan*

^{||}*Japan Science and Technology Agency, 7-3-1 Hongo, Bunkyo-ku, Tokyo 113-0033, Japan*

E-mail: michael.hayward@chem.ox.ac.uk; kage@scl.kyoto-u.ac.jp; john.mcgrady@chem.ox.ac.uk

Abstract

High-pressure X-ray diffraction measurements on the layered oxyhydrides $\text{Sr}_2\text{VO}_3\text{H}$ and $\text{Sr}_3\text{V}_2\text{O}_5\text{H}_2$ reveal that both compounds undergo a pressure-induced rock-salt to CsCl ($B1 - B2$) structural transition, similar to those observed in binary compounds (oxides, halides, chalcogenides *etc.*). This structural transition, observed at 43 and 45

GPa in $\text{Sr}_2\text{VO}_3\text{H}$ and $\text{Sr}_3\text{V}_2\text{O}_5\text{H}_2$, respectively, relieves almost all of the accumulated strain on the infinite V-O-V ladders, such that the V-O bond lengths are almost identical at 0 and 50 GPa, but are substantially compressed at intermediate pressures. The resistances of both materials with 1-dimensional VO ladders decrease with increasing pressure but, unlike SrVO_2H , which contains 2-dimensional VO_2 sheets, they remain insulating even at the highest accessible pressures. The reduction in dimensionality from planar to linear VO networks reduces the dispersion of the V-O π bands that define the band gap and so leads to insulating behavior at all measured pressures.

Keywords

Vanadium oxyhydrides, high pressure phase transition, crystallography, density functional theory

Introduction

The influence of pressure on inorganic materials is a topic of enduring interest, in part because of its relevance to the geochemistry and geophysics of the earth’s core, where pressures approach 360 GPa. Even at the rather more modest pressures accessible in the laboratory, materials can display properties quite unlike those under ambient conditions. In a recent paper¹ we explored the pressure-dependent properties of the layered oxyhydride SrVO_2H , formed by topotactic reduction of the parent perovskite phase SrVO_3 .² This 2-dimensional material contains alternating VO_2 and SrH layers, with infinite V-H-V chains running along the c axis (Figure 1). The compressibility of the *trans*- VO_4H_2 coordination sphere in this material is extremely anisotropic, and the volume change is dominated by compression along the V-H-V axis with rather smaller changes in the V-O-V plane. The compression is accompanied by a significant reduction in the measured resistance of the material, but this appears to be associated with electronic changes in the VO_2 plane rather than along the V-H chains,

despite the more pronounced structural changes in the latter. Specifically, the dispersion of both the valence and conduction bands ($V d_{xz/yz}$ and $V d_{xy}$, respectively), is dominated by V-O π interactions and so the electronic properties are influenced primarily by the strain accumulated in the V-O-V plane. The key to reducing resistance in this and related materials appears, therefore, to lie in minimising the extent to which the pressure gradient can be dissipated along directions orthogonal to the critical V-O-V bonds.

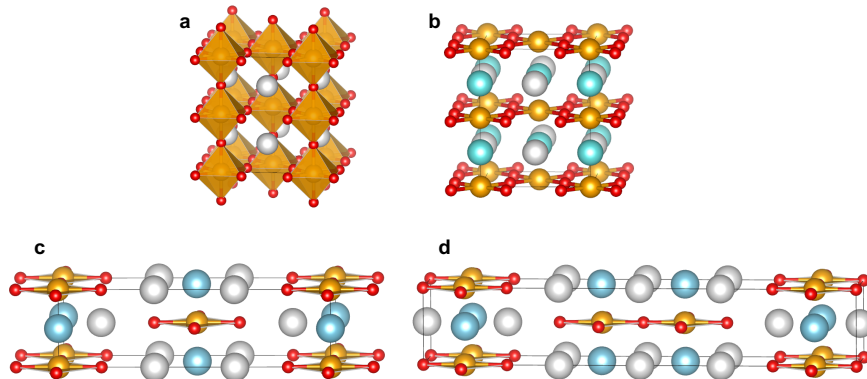


Figure 1: Crystal structure of perovskite related materials. (a) SrVO_3 , (b) SrVO_2H , (c) $\text{Sr}_2\text{VO}_3\text{H}$, (d) $\text{Sr}_3\text{V}_2\text{O}_5\text{H}_2$. White, yellow, red, and sky blue spheres denote Sr, V, O and H atoms respectively.

In this paper, we extend our studies of pressure dependence to two closely-related vanadium oxyhydrides $\text{Sr}_2\text{VO}_3\text{H}$ and $\text{Sr}_3\text{V}_2\text{O}_5\text{H}_2$,² also shown in Figure 1. These materials are generated by the topotactic reduction of the $n = 1$ and $n = 2$ Ruddlesden-Popper oxides, Sr_2VO_4 and $\text{Sr}_3\text{V}_2\text{O}_7$, which are inter-growth compounds containing perovskite and rock-salt-type layers, with the former increasing in thickness as n increases: the parent perovskite SrVO_3 can be viewed as the limiting Ruddlesden-Popper phase as $n \rightarrow \infty$. Both $\text{Sr}_2\text{VO}_3\text{H}$ and $\text{Sr}_3\text{V}_2\text{O}_5\text{H}_2$ have previously been structurally characterized at ambient pressure using neutron diffraction techniques,² and this study confirmed that the alternating perovskite/rock-salt layers are retained despite the oxide/hydride substitution. There are many similarities between these two compounds and the SrVO_2H parent: most strikingly, infinite V-H-V chains are again present, in this case running along the crystallographic b

axis. The 2-dimensional VO_2 sheets of SrVO_2H are, however, replaced by an infinite 1-dimensional V-O-V ladder along a , and alternating perovskite-like and rock-salt-like layers are stacked along the crystallographic c axis. Such a ladder structure has recently attracted attention due to the possibility of high- T_c superconductivity.³ A number of recent studies of the electronic structure of these materials have been reported, where the focus has been on the impact of correlation on the magnetic properties.⁴⁻⁸ The presence of rock-salt layers in both $\text{Sr}_2\text{VO}_3\text{H}$ and $\text{Sr}_3\text{V}_2\text{O}_5\text{H}_2$ offers a potential new dimension to the high-pressure studies, related to the so-called $B1 - B2$ transition between rock-salt ($B1$) and CsCl ($B2$) structures in binary compounds.⁹⁻¹³ The reduction in volume associated with the increase in coordination number from 6 (rock-salt) to 8 (CsCl) is sufficient to drive a structural transition at elevated pressures. The $B1 - B2$ transition is also observed in the ternary layered compounds $\text{Sr}_3\text{Fe}_2\text{O}_5$ and Sr_2CuO_3 , which have an inter-growth structure containing a rock-salt (NaCl) ordered layer.^{14,15} We may therefore anticipate that $\text{Sr}_2\text{VO}_3\text{H}$ and $\text{Sr}_3\text{V}_2\text{O}_5\text{H}_2$ will also undergo the $B1 - B2$ transition and that this may influence their physical properties. In this paper, we report high pressure synchrotron X-ray diffraction (SXRD) measurements for the two layered perovskite oxyhydrides $\text{Sr}_2\text{VO}_3\text{H}$ and $\text{Sr}_3\text{V}_2\text{O}_5\text{H}_2$, both shown in Figure 1. The structural studies are complemented by resistance measurements over the same pressure window and a detailed electronic analysis using periodic density functional theory. As for SrVO_2H , we anticipate that the ability of a pressure gradient to exert a significant influence on the resistance will depend critically on the extent to which the gradient is concentrated along the infinite V-O-V ladder, and not dissipated in orthogonal directions.

Methodology

Sample preparation

Sr_2VO_4 and $\text{Sr}_3\text{V}_2\text{O}_7$ were prepared by reduction of V^{5+} precursors under flowing hydrogen, as described previously.² Powder samples of $\text{Sr}_2\text{VO}_3\text{H}$ and $\text{Sr}_3\text{V}_2\text{O}_5\text{H}_2$ were synthesized by

topochemical reaction of these oxide phases with CaH_2 , also as reported previously.^{2,16}

High-pressure X-ray diffraction

High-pressure powder synchrotron X-ray diffraction (SXRD) experiments for $\text{Sr}_2\text{VO}_3\text{H}$ and $\text{Sr}_3\text{V}_2\text{O}_5\text{H}_2$ were performed at room temperature using the NE1A synchrotron beam line of the Photon Factory - Advanced Ring for Pulse X-rays (PF-AR) at the High Energy Accelerator Research Organization (KEK). Powder samples were loaded into a $100\text{ }\mu\text{m}$ hole of pre-indented rhenium gaskets of the diamond anvil cell (DAC). The volume of the sample space was varied using a screw, and Daphne oil 7373 was used as a pressure-transmitting medium. At each volume, the fluorescence shift of ruby chips was used to measure the pressure. To estimate the pressure distribution along the sample, several ruby chips were placed inside the hole at different distances from its center: the pressure gradient increases with pressure, but does not exceed $\pm 4\text{ GPa}$ at the highest pressures. The incident X-ray beam was monochromatized to wavelengths of $0.4181\text{ }\text{\AA}$ and $0.4175\text{ }\text{\AA}$ for $\text{Sr}_2\text{VO}_3\text{H}$ and $\text{Sr}_3\text{V}_2\text{O}_5\text{H}_2$, respectively.

High pressure resistance measurements

Four-probe AC resistance measurements for $\text{Sr}_2\text{VO}_3\text{H}$ and $\text{Sr}_3\text{V}_2\text{O}_5\text{H}_2$ were carried out using Pt electrodes. The sample/metal-gasket cavity was coated with an insulating anhydrous gypsum (CaSO_4) with epoxy. The initial sectional area and the distance between probes were about $(40 \times 40)\mu\text{m}^2$ and $30\mu\text{m}$, respectively, for both $\text{Sr}_2\text{VO}_3\text{H}$ and $\text{Sr}_3\text{V}_2\text{O}_5\text{H}_2$. The applied pressure was calibrated by means of fluorescence manometry on ruby chips placed around the sample. The resistance measurements were performed immediately after application of the pressure and also after waiting overnight following pressurisation. The results are qualitatively similar, and data for the delayed measurements are collected in Supporting information (Figure S4).

Density Functional Theory

Calculations were performed using VASP version 5.4.1,¹⁷ with the PAW-PBE methodology.^{18,19} A plane-wave energy cut-off of 600 eV was used and the Brillouin zone was sampled with k-point grids of $7 \times 7 \times 3$ for $\text{Sr}_2\text{VO}_3\text{H}$ and $7 \times 7 \times 2$ for $\text{Sr}_3\text{V}_2\text{O}_5\text{H}_2$. A Hubbard U correction of 2 eV was applied to the vanadium $3d$ orbitals, consistent with our previous study on the closely related infinite-layer phase SrVO_2H .¹ All calculations were done using a $\sqrt{2} \times \sqrt{2} \times 1$ expansion of the crystallographic unit cell, and G-type anti-ferromagnetism was imposed in the starting guess at all pressures. In all cases the resulting converged density retains the alternating spin polarization characteristic of this G-type arrangement. Calculations on the binary oxides MO , $\text{M} = \text{Ca}, \text{Sr}$ and Ba were performed using the cubic crystallographic unit cells (for both $B1$ and $B2$ forms), a plane-wave cutoff of 600 eV and an $8 \times 8 \times 8$ grid for the sampling of the first Brillouin zone. In analysing the electronic structure, we find it useful to define a hypothetical state where there is no polarization of the spin density: this is achieved simply by using a spin-restricted ansatz.

Results and Discussion

Structural studies of $\text{Sr}_2\text{VO}_3\text{H}$ and $\text{Sr}_3\text{V}_2\text{O}_5\text{H}_2$

Variable-pressure SXRD measurements

Powder SXRD patterns for the layered perovskite oxyhydrides $\text{Sr}_2\text{VO}_3\text{H}$ and $\text{Sr}_3\text{V}_2\text{O}_5\text{H}_2$ are shown in Figure 2. At the lowest pressures (3.3 GPa and 3.7 GPa for $\text{Sr}_2\text{VO}_3\text{H}$ and $\text{Sr}_3\text{V}_2\text{O}_5\text{H}_2$, respectively), the diffraction patterns can be indexed to an orthorhombic I -centered unit cell, consistent with the previous neutron diffraction study at ambient pressure² (note that in the case of $\text{Sr}_2\text{VO}_3\text{H}$, a number of weak impurity peaks are apparent in the 3 GPa dataset). The lattice parameters for $\text{Sr}_2\text{VO}_3\text{H}$ at 3.3 GPa, shown in Figure 3, are slightly compressed relative to the ambient pressure values² ($a = 3.8516 \text{ \AA}$, $b = 3.6136 \text{ \AA}$, c

$= 12.6494 \text{ \AA}$ vs 3.8881 \AA , 3.6671 \AA and 12.775 \AA , respectively). Similar trends are apparent in the comparison of the 3.7 GPa dataset for $\text{Sr}_3\text{VO}_5\text{H}_2$ (supporting information, Figure S2) with the corresponding ambient-pressure data ($a = 3.8823 \text{ \AA}$, $b = 3.6156 \text{ \AA}$, $c = 20.4437 \text{ \AA}$ vs 3.8961 \AA , 3.6806 \AA and 20.596 \AA , respectively). As the pressure is increased, the 2θ reflection peaks broaden and shift to higher angles (Figure 2), and the lattice parameters, shown as green crosses in Figure 3, contract. In the low-pressure regime ($< 40 \text{ GPa}$), the pressure dependence of the volume can be fitted well to the Birch-Murnaghan equation of state,²⁰ with bulk moduli of $K = 115(5) \text{ GPa}$ and $142(3) \text{ GPa}$, respectively, for $\text{Sr}_2\text{VO}_3\text{H}$ and $\text{Sr}_3\text{V}_2\text{O}_5\text{H}_2$. These values are slightly smaller than those for the layered perovskites $\text{Sr}_3\text{Fe}_2\text{O}_7$ ($K = 145 \text{ GPa}$)²¹ and $\text{La}_{1.4}\text{Nd}_{0.6}\text{CuO}_4$ ($K = 152 \text{ GPa}$)²² but larger than those for the layered square planar oxides Sr_2CuO_3 ($K = 99 \text{ GPa}$)¹⁵ and $\text{Sr}_3\text{Fe}_2\text{O}_5$ ($K = 94 \text{ GPa}$)¹⁴ indicating that the presence or absence of an anion in the apical site has a strong influence on the materials' properties. In the low-pressure regime ($< 40 \text{ GPa}$), a linearized Birch-Murnaghan fit to the V-O bond lengths along the infinite V-O-V chains (equal to $a/2$) gives values of $1.49(5) \times 10^{-3} \text{ GPa}^{-1}$ and $1.33(5) \times 10^{-3} \text{ GPa}^{-1}$ for the zero-pressure linear compressibility, $\beta_{\text{V-O}}$, of $\text{Sr}_2\text{VO}_3\text{H}$ and $\text{Sr}_3\text{V}_2\text{O}_5\text{H}_2$, respectively. These compare with values of $1.47(4) \times 10^{-3} \text{ GPa}^{-1}$ for SrVO_2H and $1.72(4) \times 10^{-3} \text{ GPa}^{-1}$ for the parent perovskite SrVO_3 .¹ The very similar values in all four cases suggest that the stiffness of the V-O bonds is largely independent of the global structure in these the oxyhydride phases. A fit to the variation in V-H bond lengths ($= b/2$) indicates that their compressibility, $\beta_{\text{V-H}}$, is approximately twice as great: $2.9(3) \times 10^{-3}$ and $2.5(1) \times 10^{-3} \text{ GPa}^{-1}$ for $\text{Sr}_2\text{VO}_3\text{H}$ and $\text{Sr}_3\text{V}_2\text{O}_5\text{H}_2$, respectively. The corresponding value in SrVO_2H was $3.7(2) \times 10^{-3} \text{ GPa}^{-1}$, confirming that the greater compressibility of the V-H bond is also a general feature of vanadium oxyhydride family. The presence of distinct rock-salt and VO blocks along c makes it more difficult to interpret the pressure dependence of this parameter in terms of specific bond lengths: we return to this point in the computational analysis.

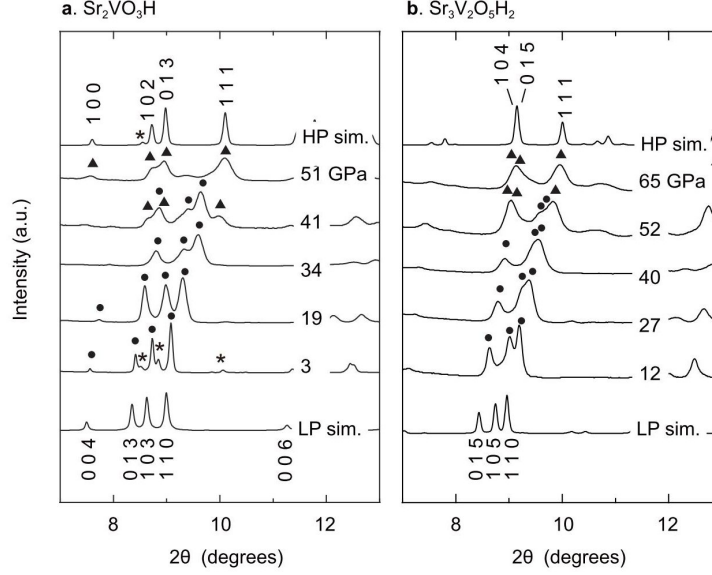


Figure 2: Powder SXRD patterns of (a) $\text{Sr}_2\text{VO}_3\text{H}$, (b) $\text{Sr}_3\text{V}_2\text{O}_5\text{H}_2$ at room temperature under high pressures. For each specimen, the patterns can be indexed using the orthorhombic I -centered cell for $P < P_s$ and the orthorhombic A -centered cell for $P > P_s$. Simulation patterns of the low pressure phase (LP sim.) and the high pressure phase (HP sim.) are shown for comparison. Peaks marked by circles and triangles, respectively, represent the low and high pressure phases. Peaks with asterisks denote unknown impurity.

Just above 40 GPa, a distinct change in the diffraction patterns occurs for both $\text{Sr}_2\text{VO}_3\text{H}$ and $\text{Sr}_3\text{V}_2\text{O}_5\text{H}_2$, marking a discontinuous change in the cell volume and also a change in the reflection conditions, from an orthorhombic I -centered to an orthorhombic A -centered lattice. Very similar pressure-induced transitions, from orthorhombic I -centered to A -centered unit cells, have been observed in the rock-salt inter-growth phases A_2BO_3 ($\text{A} = \text{Sr}, \text{Ca}, \text{B} = \text{Cu}, \text{Pd}$)¹⁵ and $\text{Sr}_3\text{Fe}_2\text{O}_5$ ¹⁴ and traced to a phase shift of the neighboring octahedral chains (ladders) along the b axis, from $(1/2, 1/2, 1/2)$ at low pressure to $(1/2, 0, 1/2)$ at high pressure (the $B1 - B2$ transition). Simulation of the diffraction patterns for the high-pressure phases of $\text{Sr}_2\text{VO}_3\text{H}$ and $\text{Sr}_3\text{V}_2\text{O}_5\text{H}_2$ are entirely consistent with analogous transitions, as shown for $\text{Sr}_2\text{VO}_3\text{H}$ in the upper part of Figure 3. The critical transition pressures, P_s (the point where the volume fractions of the two phases are equal, Fig. S3 in the Supporting Information) are 45 and 43 GPa for $\text{Sr}_2\text{VO}_3\text{H}$ and $\text{Sr}_3\text{V}_2\text{O}_5\text{H}_2$, respectively.

The unit cell for the A -centered structure, shown in Figure 3, can be separated into distinct

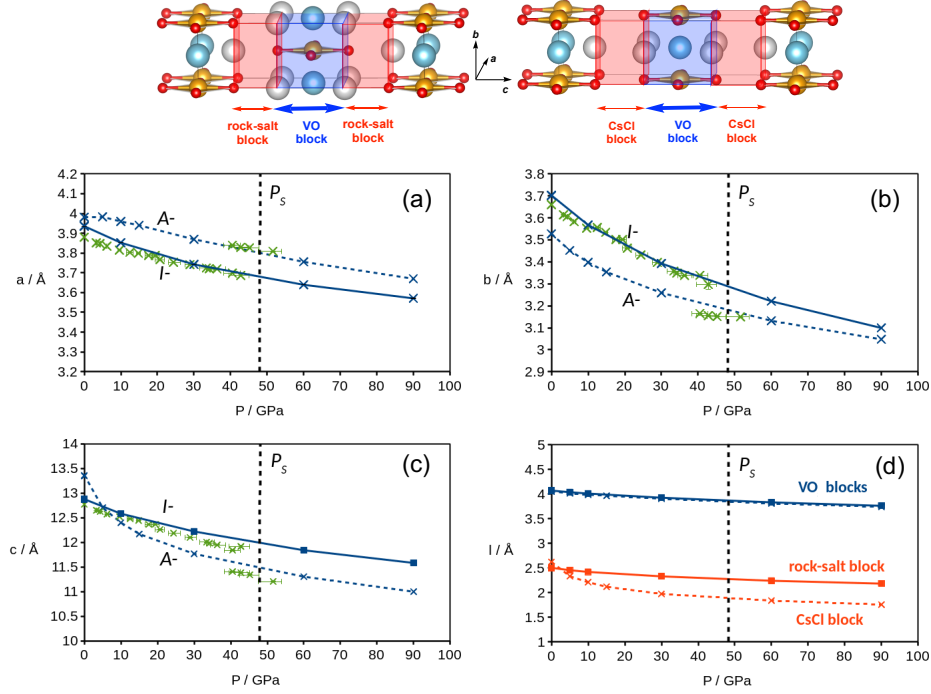


Figure 3: (a)-(c) Measured (green) and computed (blue) lattice parameters, a , b and c of $\text{Sr}_2\text{VO}_3\text{H}$, respectively. Solid and dashed lines refer to the I - and A - form, respectively. The black dashed line marked P_s marks the computed transition pressure. (d) Decomposition of the variation in c into separate contributions from the VO and rock-salt/CsCl blocks

VO blocks and CsCl-like, rather than rock-salt-like, blocks. Otherwise, the A -centered high-pressure form retains many of the features of the I -centered analogue: infinite V-O-V and V-H-V chains remain aligned along the a and b axes, respectively. The switch from the I - to A -centered phase at the critical pressure is marked by abrupt changes in all three lattice parameters. Most strikingly, c drops from ~ 11.9 Å just before the transition to ~ 11.4 Å just after it. There is a somewhat smaller compression along b from ~ 3.3 Å above (P_s) to ~ 3.15 Å below it (note the different scales used for a , b and c). In contrast, there is an expansion along a (~ 3.69 Å to ~ 3.84 Å) at the critical pressure, which restores the V-O bond lengths almost back to their ambient pressure value of 3.8516 Å. The behaviour of the high-pressure structure of $\text{Sr}_3\text{V}_2\text{O}_5\text{H}_2$ is very similar, and is shown in supporting information, Figure S2. The relationship between $\log(P_s)$ and the radius ratio, R_A/R_O , for $\text{Sr}_2\text{VO}_3\text{H}$, $\text{Sr}_3\text{V}_2\text{O}_5\text{H}_2$ is shown in Figure 4, along with the corresponding values for other known binary oxides

and inter-growth phases. It is known that the logarithm of the $B1 - B2$ structural transition pressure, $\log(P_s)$, in binary compounds depends linearly on the ratio of the ionic radii R_A/R_X ,²³⁻²⁵ and this correlation extends to the two-dimensional inter-growth compounds $(AO)(AMO_2)_n$ ($A = \text{Sr, Ca}$; $M = \text{transition metal}$; $n = 1, 2$), composed of alternating rock-salt (AO) and square planar (AMO_2) layers (Figure 4).¹⁵ The fact that $\log(P_s)$ is relatively insensitive to the identity of the transition metal¹⁵ in these inter-growth compounds suggests that it is the rock-salt/CsCl block that dominates the pressure dependence. Like the bulk modulus, the critical pressure is also strongly dependent on the electron density at the apical sites (*i.e.* those occupied by hydrides in $\text{Sr}_2\text{VO}_3\text{H}$ and $\text{Sr}_3\text{V}_2\text{O}_5\text{H}_2$), as illustrated by the much higher values for $\text{Sr}_3\text{Ir}_2\text{O}_7$ ²⁶ and $\text{LaSrNiO}_{3.4}$,¹⁴ where these sites are fully and $\sim 40\%$ occupied, respectively. Assuming that a similar linear correlation exists between $\log(P_s)$ and the radius ratio, R_A/R_O , for the oxyhydrides $\text{Sr}_2\text{VO}_3\text{H}$ and $\text{Sr}_3\text{V}_2\text{O}_5\text{H}_2$, their positions in the plot suggest that the presence of hydride ligands in the apical sites (with 100% occupation) has an effect broadly comparable to an oxide site with approximately 40% occupation. This is consistent with other observations which show that hydride ions are significantly more compressible than oxide ions.¹

Pressure-dependent resistance of $\text{Sr}_2\text{VO}_3\text{H}$ and $\text{Sr}_3\text{V}_2\text{O}_5\text{H}_2$

Figure 5 shows the resistance of $\text{Sr}_2\text{VO}_3\text{H}$ and $\text{Sr}_3\text{V}_2\text{O}_5\text{H}_2$ as a function of applied pressure. The corresponding data set for SrVO_2H , reported previously,¹ is also shown for comparison. The resistances of $\text{Sr}_2\text{VO}_3\text{H}$ and $\text{Sr}_3\text{V}_2\text{O}_5\text{H}_2$ show very similar behavior, decreasing significantly with increasing pressure, but neither plot shows any discontinuity coincident with the crystallographic phase transitions described above. It is possible that the absence of such a discontinuity reflects the slow kinetics of the phase transition, but control experiments on $\text{Sr}_3\text{V}_2\text{O}_5\text{H}_2$ where an overnight delay was introduced between pressurization (at room temperature) and measurement of resistance gave qualitatively similar results (Figure S4). The decrease in resistance with pressure is broadly similar to the behaviour of SrVO_2H but at

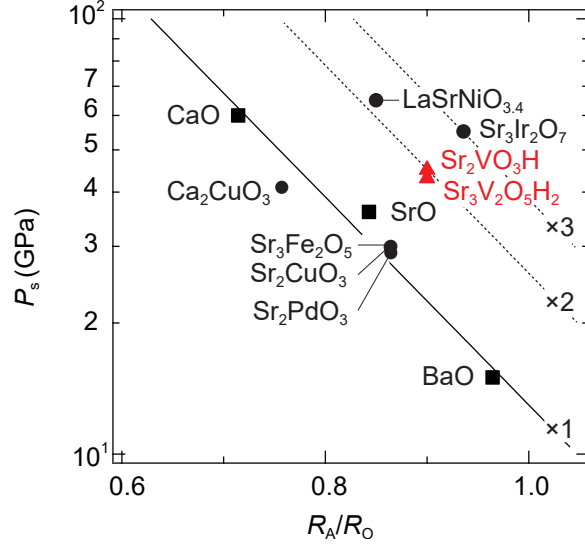


Figure 4: $\log(P_s)$ of the *B1-B2* structural transition vs the ratio of the A-site ion radius (R_A) to the oxide ion radius (R_O). R_A in 6-, 7-, 8-, 8-, and 9-fold coordination are used,²⁷ respectively, for AO, A_2MO_3 ($Sr_3Fe_2O_5$), $LaSrNiO_{3.4}$, oxyhydrides, and $Sr_3Ir_2O_7$. P_s for binary systems AO (black squares) and for inter-growth oxides (black circles) are taken from the references^{13,28,29}

each pressure the gradient $\Delta R/\Delta T$ remains negative for both Sr_2VO_3H and $Sr_3V_2O_5H_2$ even up to highest accessible pressures (48 and 57 GPa respectively). In $SrVO_2H$, in contrast, the gradient is very close to zero at elevated pressures, behaviour that is characteristic of a semi-metal with a zero band gap. Thus there appears to be a significant difference between the 1-dimensional phases considered here and their 2-dimensional analogue, $SrVO_2H$, in so much as the former appear to remain band-gap insulators at all accessible pressures.

DFT analysis of the electronic structure of Sr_2VO_3H and $Sr_3V_2O_5H_2$

Having discussed the experimental data in some detail, we now turn to density functional theory (DFT) to provide support for the interpretations set out in the previous paragraphs. Specifically, the computational analysis will provide insight into three important issues that cannot be resolved by the experimental data in isolation. Firstly, the experiments can, by definition, probe only the structure of the phase that is present under a given set of conditions. They are, therefore, blind to the *A*-centered phase at low pressure and to the *I*-centered phase

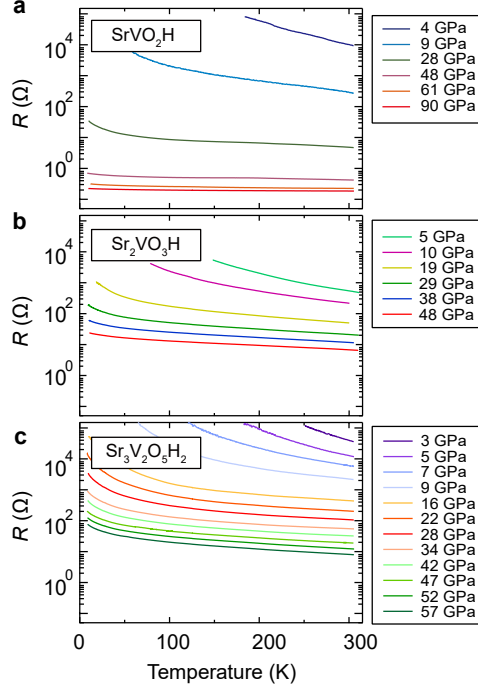


Figure 5: Electrical resistances under pressure. Temperature dependence of resistance R at various pressures for (a) SrVO_2H , (b) $\text{Sr}_2\text{VO}_3\text{H}$, (c) $\text{Sr}_3\text{V}_2\text{O}_5\text{H}_2$.

at high pressure. The computational model allows us to explore how both structures vary across the entire pressure range. Secondly, the experimental data do not provide atomic-level resolution, as a result of which we cannot break down the compression along c into separate components due to changes in the VO_2 and rock-salt/CsCl layers. Finally, through the density of states around the Fermi level, we hope to establish a direct connection between the structural parameters shown in Figure 3 and the resistance data in Figure 5.

The variations in the computed lattice parameters, a , b and c for the I - and A -centered phases of $\text{Sr}_2\text{VO}_3\text{H}$ are shown as full and dashed blue lines, respectively, in Figure 3(a)-(c). The corresponding data for $\text{Sr}_3\text{V}_2\text{O}_5\text{H}_2$ are shown in supporting information, Figure S5. There is a striking correspondence between the calculated values and the experimental data (green crosses) for all three parameters, a , b and c . The critical pressure can be defined as the point where the calculated enthalpy change, $\Delta H_s = \Delta E_s + P\Delta V_s$, equals zero, and the resulting values of 48 GPa and 50 GPa for $\text{Sr}_2\text{VO}_3\text{H}$ and $\text{Sr}_3\text{V}_2\text{O}_5\text{H}_2$, respectively, are in

excellent agreement with experiment. Perhaps the most striking feature of the curves is the c axis, which, at ambient pressure, is ~ 0.5 Å *longer* for the A -centered unit cell. However, even a very modest increase in pressure has a dramatic impact on the value of c for the A -centered lattice, such that it falls below the I -centered structure at ~ 5 GPa and by the time this phase becomes accessible to the experiment at the critical pressure of 45 GPa, c is almost 0.5 Å *shorter* in the A -centered form. We can obtain more information by breaking up the variations in c into separate contributions from the VO_2 layers and the rock-salt/CsCl layers, which are shown in red and blue in Figure 3(d) (note that value of c is simply twice the sum of the two components). This decomposition reveals that the different compressibilities of the two structures are caused solely by differences in the rock-salt/CsCl layers: the CsCl block in the A -centered lattice is compressed by ~ 1.0 Å over the 90 GPa pressure range while the corresponding change in the rock-salt layer is only ~ 0.3 Å. The VO blocks in the two cases are, in contrast, almost indistinguishable from each other and, moreover, are not strongly dependent on pressure. Exactly the same patterns emerge in the $\text{Sr}_3\text{V}_2\text{O}_5\text{H}_2$ case shown in supporting information, Figure S5, except that the compressibility of the VO block, with four V-O bonds along the c axis, is now almost exactly double the compressibility of the VO block in $\text{Sr}_2\text{VO}_3\text{H}$ where there are only two such bonds. This reinforces the view that the V-O bonds are essentially invariant to the wider environment. The origin of the very different compressibilities along c in the two structures can be traced to the nature of the nearest-neighbour interactions in the rock-salt/CsCl blocks. In the I -centered form, the nearest-neighbour interactions along c are between ions of opposite charge (O/Sr), and the Sr-O separation of 2.50 Å is below the sum of the respective ionic radii ($r(\text{Sr}) + r(\text{O}) = 2.58$ Å) even at 0 GPa. Further compression along c is therefore opposed by the steep repulsive potential imposed by the ionic cores. In the A -centered analogue, in contrast, the nearest neighbours have the same charge (O/O in the upper and lower layers, Sr/Sr in the middle layer). Moreover, the nearest neighbours in the A -centered form are offset along the a axis, such that the separation between the oxide ions is 3.29 Å, much greater than the

sum of the ionic radii (2.52 Å). As a result, compression is opposed only by the relatively shallow increase in potential energy imposed by the long-range electrostatic repulsions, and is much easier as a consequence. Just below P_s the pressure gradient in the I -centered form is distributed approximately equally over the three orthogonal lattice directions, a , b and c , but above the transition point the gradient is absorbed mostly by compression along c , relieving almost all of the compression that had previously accumulated along the V-O bonds along a .

In order to explore the link between structure and resistance, we have plotted the density of states, projected onto the V $3d$ orbitals, for both the I - and A -centered lattices at ambient pressure and at 60 GPa in Figure 6. The corresponding data for SrVO_2H are also shown for comparison. The projection of the DOS presents a minor problem in that the V-H-V chain is aligned along the crystallographic c axis in SrVO_2H whereas it is aligned along b in $\text{Sr}_2\text{VO}_3\text{H}$ and $\text{Sr}_3\text{V}_2\text{O}_5\text{H}_2$. To facilitate the comparison between the three materials, we therefore define a common local axis system where in all cases the V-H-V chain is aligned along the z axis and the infinite V-O-V ladder is aligned along x . The ambient pressure plot for SrVO_2H is very typical of a lattice of anti-ferromagnetically (AFM) coupled V(III) ions (d^2). The calculated spin densities at V are $\pm 1.5 \mu_B$, and the majority-spin components of the V $d_{xz/yz}$ orbitals (green and red) are both occupied and degenerate in tetragonal symmetry while the d_{xy} band (purple) is destabilized by strong in-plane V-O π interactions and lies above the Fermi level. Very similar features emerge for both I - and A - forms of $\text{Sr}_2\text{VO}_3\text{H}$, except that now the degeneracy of the bands below the Fermi level is lifted due to inequivalence of the a and c axes. The dispersion along a (the infinite V-O-V ladder) remains pronounced (red) but the intervening rock-salt/CsCl blocks prevent dispersion along c (green). The d_{xy} band above the Fermi level is also much narrower in $\text{Sr}_2\text{VO}_3\text{H}$ than in SrVO_2H , again reflecting the contrast between a 2-dimensional VO_2 lattice and a 1-dimensional V-O-V chain. At 60 GPa, the compression of SrVO_2H in the ab plane drives an increase in the dispersion of both the V $d_{xz/yz}$ and V d_{xy} bands, to the extent that they meet at the Fermi level,

effectively eliminating the band gap. The DOS at this point is typical of a semi-metallic state, where the resistance is independent of temperature. Turning to the 60 GPa DOS of the *I*- and *A*- forms of $\text{Sr}_2\text{VO}_3\text{H}$, the same general features are apparent: the DOS broadens, most obviously for the red ($\text{V } d_{xz}$) and purple ($\text{V } d_{xy}$) bands where there is strong dispersion along the infinite V-O-V ladder aligned along *a*. Just as the lower dimensionality of $\text{Sr}_2\text{VO}_3\text{H}$ compared to SrVO_2H led to narrower bands in the former at ambient pressure, it also means that the bands are less sensitive to pressure, and a clear band-gap remains even at 60 GPa. Differences between the *I*- and *A*-centered forms are marginal, but there is slightly greater dispersion in the red d_{xz} band in the *I*-centered form, such that the top of this band defines the Fermi level whereas it is the green d_{yz} band in the *A*-centered analogue. The variations in DOS across the three structures suggest that the presence of a band gap in the high-pressure forms of both $\text{Sr}_2\text{VO}_3\text{H}$ or $\text{Sr}_3\text{V}_2\text{O}_5\text{H}_2$, as measured by the negative gradient of the resistance *vs* temperature plot, is primarily due to the presence of an infinite 1-dimensional VO ladder rather than the 2-dimensional VO_2 sheet in SrVO_2H . The effect of the transition from the *I*- to *A*-centered phases seems to be of secondary importance because the band gap at 60 GPa is only very marginally larger than in the *A*-centered form. This observation is consistent with the absence of any marked discontinuity at the critical pressure in the resistance *vs* temperature curves shown in Figure 5.

In related studies on the high-pressure behaviour of $\text{Sr}_3\text{Fe}_2\text{O}_5$,¹⁴ a transition to a ferromagnetic (FM) metallic state was observed. In the vanadium systems of interest here all FM states were found to lie 0.5 – 1.0 eV above the AFM ground state across the entire pressure range. We have, however, been able to locate diamagnetic, truly metallic states where the electrons are entirely delocalized by performing an additional series of calculations using spin-restricted density functional theory, where polarisation of the α and β orbitals is prevented by construction. The metallic state proves to be less stable than the spin-polarized AFM forms described above at all pressures, as shown in Figure S7 in the Supporting Information, but in SrVO_2H the separation goes from 3 eV/unit cell at ambient pressure to

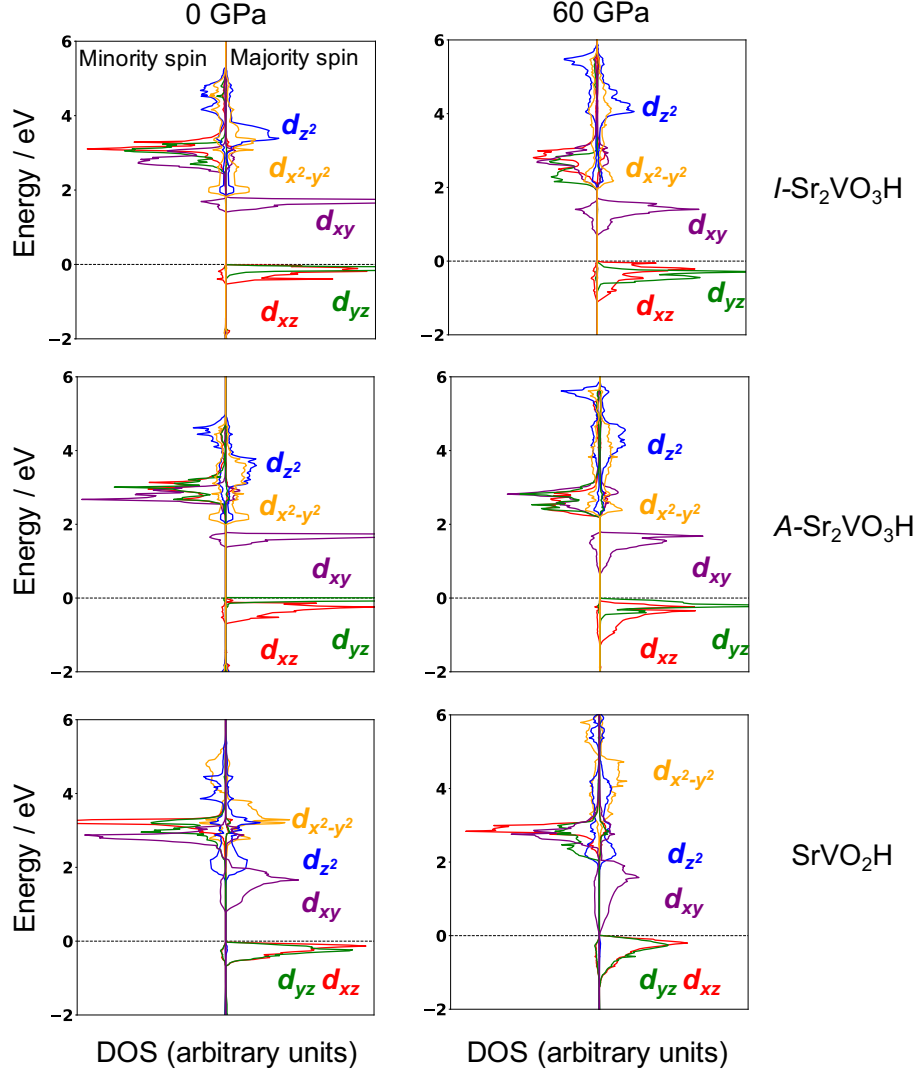


Figure 6: Vanadium PDOS plots for $I\text{-Sr}_2\text{VO}_3\text{H}$, $A\text{-Sr}_2\text{VO}_3\text{H}$ and SrVO_2H at 0 and 60 GPa, and enthalpy differences between the anti-ferromagnetic and diamagnetic states of vanadium oxyhydrides as functions of pressure.

only 1.1 eV/unit cell at 90 GPa. We note here that in a previous publication we reported this diamagnetic metallic state as the ground state of SrVO_2H at 60 GPa. Subsequent work has revealed the slightly more stable semi-metallic but still AFM configuration shown in the DOS plot in Figure 6. The separation between metallic and AFM states is always largest for $\text{Sr}_2\text{VO}_3\text{H}$: the values vary from ~ 4 eV/unit cell at 0 GPa to ~ 3 eV/unit cell at 90 GPa. The 1-dimensional $\text{Sr}_2\text{VO}_3\text{H}$ ladder is therefore further away from the metallic crossover than 2-dimensional SrVO_2H ladder at all pressures, consistent with the larger band gap and the

measured resistance data.

Summary and conclusions

In this paper we have analyzed the influence of pressure on both the structure and resistance of two 1-dimensional vanadium oxyhydride compounds, $\text{Sr}_2\text{VO}_3\text{H}$ and $\text{Sr}_3\text{V}_2\text{O}_5\text{H}_2$, and compared them to the 2-dimensional parent, SrVO_2H . At ambient pressure, both compounds adopt an *I*-centered inter-growth lattice with VO_2H ladders separated by rock-salt blocks. At pressures above ~ 50 GPa, however, a *B1* – *B2*-type structural transition occurs, generating an *A*-centered orthorhombic phase where the rock-salt blocks are replaced by CsCl-like units. Resistance measurements on powder samples suggest that although the band gap decreases with increasing pressure, insulating behaviour is maintained across the entire accessible pressure range. This *B1* – *B2* transition has the effect of relieving much of the strain that accumulates on the infinite V-O-V ladder in the 0-45 GPa window, absorbing it in the highly compressible CsCl blocks of the *A*-centered lattice. As a result, just above the critical pressure (around 45 GPa) the V-O bonds along the infinite ladders are only very marginally shorter than they are at ambient pressure. The reduction in dimensionality of the V-O lattice from 2 in SrVO_2H to 1 in $\text{Sr}_2\text{VO}_3\text{H}$ and $\text{Sr}_3\text{V}_2\text{O}_5\text{H}_2$ limits the dispersion of the V *3d* bands, such that they remain semi-conductors even at elevated pressures. Structural optimizations performed using DFT indicate that the critical feature of the pressure-dependent behaviour is the very high compressibility of the CsCl blocks in the *A*-centered lattice compared to their rock-salt counterparts in the *I*-centered phase, which leads to a rapid reduction in volume and hence stabilization of the former at elevated pressures. The very high compressibility along the *c* axis absorbs most of the pressure gradient, and as a result the strain accumulated in the V-O ladders is comparatively modest. Therefore, whilst the pressure-induced structural changes in $\text{Sr}_2\text{VO}_3\text{H}$ and $\text{Sr}_3\text{V}_2\text{O}_5\text{H}_2$ are more dramatic than those in SrVO_2H in the

sense that a lattice rearrangement occurs, the impact on the underlying electronic structure of the vanadium centers is rather modest due to the buffering effect of the rock-salt/CsCl inter-growth regions.

Acknowledgement

The work was supported by CREST, the Japan Society for the Promotion of Science (JSPS) Core-to-Core Program (A) Advanced Research Networks, The Project of Creation of Life Innovation Materials for Interdisciplinary and International Researcher Development of the Ministry of Education, Culture, Sports, Science and Technology, Japan and JSPS KAKENHI (JP16H06438, JP16H6439, JP16H6440 and JP16H06033). High-pressure synchrotron radiation experiments were performed under the approval of the Photon Factory Program Advisory Committee (No. 2017G008, 2019G021). We thank Taku Okada, Daisuke Nishio-Hamane, Hirotada Gotou, Takumi Kikegawa, and Nobumasa Funamori for their support of the high-pressure XRD measurement. MAP thanks CONACYT and the Balliol College, Oxford for a scholarship. HWTM thanks the EPSRC for support through the Centre for Doctoral Training, Theory and Modelling in Chemical Sciences, under grant EP/L015722/1, and the Radcliffe scholarship fund at University College, Oxford.

Supporting Information Available

X-ray diffraction data for $\text{Sr}_2\text{VO}_3\text{H}$ and $\text{Sr}_3\text{V}_2\text{O}_5\text{H}_2$ (Figures S1 and S2). Volume fractions for the *I*- and *A*-centered phases of $\text{Sr}_2\text{VO}_3\text{H}$ and $\text{Sr}_3\text{V}_2\text{O}_5\text{H}_2$ as a function of pressure (Figure S3). Measured and calculated lattice parameters for $\text{Sr}_3\text{V}_2\text{O}_5\text{H}_2$ as a function of pressure (Figure S4). Resistance measurements on $\text{Sr}_3\text{V}_2\text{O}_5\text{H}_2$ after an overnight delay to allow for slow phase equilibration (Figure S5). Summary of computed structures for $\text{Sr}_2\text{VO}_3\text{H}$ and $\text{Sr}_3\text{V}_2\text{O}_5\text{H}_2$ (Tables S1-4) and Density of States data for $\text{Sr}_3\text{V}_2\text{O}_5\text{H}_2$ (Figure S6). Computed enthalpy differences between diamagnetic and antiferromagnetic states for SrVO_2H , $\text{Sr}_2\text{VO}_3\text{H}$

and $\text{Sr}_3\text{V}_2\text{O}_5\text{H}_2$ as a function of pressure (Figure S7).

This material is available free of charge via the Internet at <http://pubs.acs.org/>.

References

- (1) Yamamoto, T.; Zeng, D. H.; Kawakami, T.; Arcisauskaite, V.; Yata, K.; Patino, M. A.; Izumo, N.; McGrady, J. E.; Kageyama, H.; Hayward, M. A. The role of π -blocking hydride ligands in a pressure-induced insulator-to-metal phase transition in SrVO_2H . *Nat. Commun.* **2017**, *8*.
- (2) Romero, F. D.; Leach, A.; Möller, J. S.; Foronda, F.; Blundell, S. J.; Hayward, M. A. Strontium vanadium oxide-hydrides: "square-planar" two-electron phases. *Angew. Chem., Int. Ed.* **2014**, *53*, 7556–7559.
- (3) Kuroki, K.; Higashida, T.; Arita, R. High-T-c superconductivity due to co-existing wide and narrow bands: a fluctuation exchange study of the Hubbard ladder as a test case. *Phys. Rev. B* **2005**, *72*, 4.
- (4) Ochi, M.; Kuroki, K. Effective interaction for vanadium oxyhydrides $\text{Sr}_{n+1}\text{V}_n\text{O}_{2n+1}\text{H}_n$ ($n = 1$ and $n \rightarrow \infty$): A constrained-RPA study. *Phys. Rev. B* **2019**, *99*, 19.
- (5) Wei, Y.; Gui, H.; Li, X.; Zhao, Z.; Zhao, Y.-H.; Xie, W. The effect of hydrogen ordering on the electronic and magnetic properties of the strontium vanadium oxyhydride. *J. Phys.: Condens. Matter* **2015**, *27*, 206001.
- (6) Liu, K.; Hou, Y.; Gong, X.; Xiang, H. Orbital delocalization and enhancement of magnetic interactions in perovskite oxyhydrides. *Sci. Rep.* **2016**, *6*.
- (7) Bang, J.; Matsuishi, S.; Hiraka, H.; Fujisaki, F.; Otomo, T.; Maki, S.; Yamaura, J.; Kumai, R.; Murakami, Y.; Hosono, H. Hydrogen ordering and new polymorph of layered perovskite oxyhydrides: $\text{Sr}_2\text{VO}_{4-x}\text{H}_x$. *J. Am. Chem. Soc.* **2014**, *136*, 7221–7224.

- (8) Bang, J.; Matsuishi, S.; Maki, S.; Yamaura, J.; Hiraishi, M.; Takeshita, S.; Yamauchi, I.; Kojima, K. M.; Hosono, H. Low dimensionalization of magnetic ordering in Sr_2VO_4 by hydride ion substitution. *Phys. Rev. B* **2015**, *92*, 7.
- (9) Sims, C. E.; Barrera, G. D.; Allan, N. L.; Mackrodt, W. C. Thermodynamics and mechanism of the B1-B2 phase transition in group-I halides and group-II oxides. *Phys. Rev. B* **1998**, *57*, 11164–11172.
- (10) Potzel, O.; Taubmann, G. The pressure induced B1-B2 phase transition of alkaline halides and alkaline earth chalcogenides: a first principles investigation. *J. Solid State Chem.* **2011**, *184*, 1079–1084.
- (11) Cinthia, A. J.; Priyanga, G. S.; Rajeswarapalanichamy, R.; Iyakutti, K. Structural, electronic and mechanical properties of alkaline earth metal oxides MO (M=Be, Mg, Ca, Sr, Ba). *J. Phys. Chem. Solids* **2015**, *79*, 23–42.
- (12) Mammone, J. F.; Mao, H. K.; Bell, P. M. Equations of state of CaO under static pressure conditions. *Geophys. Res. Lett.* **1981**, *8*, 140–142.
- (13) Sato, Y.; Jeanloz, R. Phase transition in SrO. *J. Geophys. Res.* **1981**, *86*, 1773–1778.
- (14) Yamamoto, T.; Tassel, C.; Kobayashi, Y.; Kawakami, T.; Okada, T.; Yagi, T.; Yoshida, H.; Kamatani, T.; Watanabe, Y.; Kikegawa, T.; Takano, M.; Yoshimura, K.; Kageyama, H. Pressure-induced structural, magnetic, and transport transitions in the two-legged ladder $\text{Sr}_3\text{Fe}_2\text{O}_5$. *J. Am. Chem. Soc.* **2011**, *133*, 6036–6043.
- (15) Yamamoto, T.; Kobayashi, Y.; Okada, T.; Yagi, T.; Kawakami, T.; Tassel, C.; Kawasaki, S.; Abe, N.; Niwa, K.; Kikegawa, T.; Hirao, N.; Takano, M.; Kageyama, H. B1-to-B2 structural transitions in rock salt intergrowth structures. *Inorg. Chem.* **2011**, *50*, 11787–11794.

- (16) Bridges, C. A.; Darling, G. R.; Hayward, M. A.; Rosseinsky, M. J. Electronic structure, magnetic ordering, and formation pathway of the transition metal oxide hydride $\text{LaSrCoO}_3\text{H}_{0.7}$. *J. Am. Chem. Soc.* **2005**, *127*, 5996–6011.
- (17) Kresse, G.; Furthmüller, J. Efficient iterative schemes for ab initio total-energy calculations using a plane-wave basis set. *Phys. Rev. B* **1996**, *54*, 11169–11186.
- (18) Blöchl, P. E. Projector Augmented Wave Method. *Phys. Rev. B* **1994**, *50*, 17953–17979.
- (19) Perdew, J. P.; Burke, K.; Ernzerhof, M. Generalized gradient approximation made simple. *Phys. Rev. Lett.* **1996**, *77*, 3865–3868.
- (20) Birch, F. The Effect of Pressure Upon the Elastic Parameters of Isotropic Solids, According to Murnaghan’s Theory of Finite Strain. *J. Appl. Phys.* **1938**, *9*, 279–288.
- (21) Rozenberg, G. K.; Machavariani, G. Y.; Pasternak, M. P.; Milner, A. P.; Hearne, G. R.; Taylor, R. D.; Adler, P. Pressure-induced metallization of the perovskite $\text{Sr}_3\text{Fe}_2\text{O}_7$. *Phys. Status Solidi B* **1999**, *211*, 351–357.
- (22) Wilhelm, H.; Cros, C.; Arrouy, F.; Demazeau, G. Pressure induced structural transition in the solid-solution $\text{La}_{2-x}\text{Nd}_x\text{CuO}_4$ for $x=0.6, 0.7, 1.2$, and 1.5 . *J. Solid State Chem.* **1996**, *126*, 88–94.
- (23) Syassen, K. Pressure-induced structural transition in SrS . *Phys. Status Solidi A* **1985**, *91*, 11–15.
- (24) Ekbundit, S.; Chizmeshya, A.; LaViolette, R.; Wolf, G. H. Theoretical and experimental investigation of the equations of state and phase stabilities of MgS and CaS . *J. Phys.: Condens. Matter* **1996**, *8*, 8251–8265.
- (25) Narayana, C.; Nesamony, V. J.; Ruoff, A. L. Phase transformation of BeS and equation-of-state studies to 96 GPa. *Phys. Rev. B* **1997**, *56*, 14338–14343.

- (26) Donnerer, C.; Feng, Z.; Vale, J. G.; Andreev, S. N.; Solovyev, I. V.; Hunter, E. C.; Hanfland, M.; Perry, R. S.; Ronnow, H. M.; McMahon, M. I.; Mazurenko, V. V.; McMorro, D. F. Pressure dependence of the structure and electronic properties of $\text{Sr}_3\text{Ir}_2\text{O}_7$. *Phys. Rev. B* **2016**, *93*.
- (27) Shannon, R. D. Revised effective ionic radii and systematic studies of interatomic distances in halides and chalcogenides. *Acta Crystallogr. Sect. A: Cryst. Phys., Diff., Theor. Gen. Crystallogr.* **1976**, *32*, 751–767.
- (28) Liu, L.; Bassett, W. A. Effect of pressure on the crystal structure and lattice parameters of BaO. *J. Geophys. Res.* **1972**, *77*, 4934.
- (29) Jeanloz, R.; Ahrens, T. J.; Mao, H. K.; Bell, P. M. B1-B2 transition in calcium oxide from shock wave and diamond cell experiments. *Science* **1979**, *206*, 829–830.

Graphical TOC Entry

